nature communications

Article

https://doi.org/10.1038/s41467-026-76196-x

# Quenched-in shear transformation zones and Schmid-like visco-elastic creep in metallic glass

Received: 24 December 2024

Accepted: 21 July 2026

Published online: 05 August 2026

Check for updates

Yu Chen[1,2,5], Xinyu Luo[1,2,5], Xinyu Ding[1,2,5], Song Ling Liu[3] ✉, Weihua Wang[4] & Yong Hao Sun[1,2] ✉

The absence of periodic atomic arrangement makes it difficult to detect microscopic defects in metallic glasses, yet their roles in macroscopic shape change are prominent. Motivated by probing defects mechanically, we perform stepwise tensile creep at ambient temperature on as-spun metallic-glass ribbons that show structural anisotropy in selected area electron diffraction. The main discovery is a non-linear strain response in which the segmentally added stress causes the creep strain to initially decrease before increasing. Some strain components quickly revert after stress removal when cyclic creep is conducted, but others do not. Only the first cycle exhibits this slower-than-creep reversal; subsequent cycles have reversible strain components. The non-linearity and slow reversal are eliminated after annealing. No measurable relaxation-enthalpy change is detected within the present fast-differential-scanning-calorimetry sensitivity, suggesting that the low-stress response is not dominated by stored rejuvenation. Molecular-dynamics simulation replicates the strain responses under stepwise and cyclic creep, revealing different non-affine responses of atoms at low and high stresses. The observed behavior can be interpreted within a unified framework involving the depletion of a finite quenched-in shear-transformation-zone population together with the increasing contribution of stress-activated shear-transformation-zones. These results support an orientation-dependent, Schmid-like interpretation of low-stress visco-elastic creep in metallic glass ribbons.

Metallic glasses (MGs) are a class of advanced materials known for their high resilience[1] and, in certain compositions, excellent soft magnetic properties that enable highly efficient energy conversion[2–4]. A recently-developed FeCo-based MG/nano-crystalline alloy exhibits an exceptionally high saturation magnetic flux density of 1.94 T and a coercivity as low as 4.3 A $m^{-1}$ (Ref. 5). Motors employing Fe-based MG/nano-crystalline alloys for iron cores have been utilized for commercial electric vehicles. Nevertheless, embrittlement remains a critical issue in the manufacturing of such cores[6]. Annealed MG ribbons can fracture under bending at relatively large radii of curvature ($R$), corresponding to bending strains ($=\frac{d}{2R}$) well below the 2% elastic strain limit of MGs[7]. This has sparked renewed and strong interest in understanding the embrittlement of MG ribbons, especially within their nominally elastic regime.

As-cast MG rods often exhibit higher compressive plasticity compared to their annealed counterparts[8]. MGs with high plasticity

[1]Institute of Physics, Chinese Academy of Sciences, Beijing, China. [2]School of Physical Sciences, University of Chinese Academy of Sciences, Beijing, China. [3]Advanced Interdisciplinary Science Research (AiR) Center, Ningbo Institute of Materials Technology and Engineering, Chinese Academy of Sciences, Ningbo, Zhejiang, China. [4]Dongguan Institute of Materials Science and Technology, Dongguan, Guangdong, China. [5]These authors contributed equally: Yu Chen, Xinyu Luo, Xinyu Ding. ✉e-mail: liusl95@outlook.com; ysun58@iphy.ac.cn

exhibit diffuse, low-amplitude serrations on the stress-strain curves of as-cast rods, while those with low plasticity have fewer, higher-magnitude serrations[9]. The sluggish stick-slip motion of shear bands[10] allows for plasticity and prevents catastrophic failure, which is frequently observed in annealed samples[11]. The fracture surfaces show shallower vein patterns after sub-$T_g$ ($T_g$ being the glass-transition temperature) annealing, and there is no shear banding at the notch root[12]. As-cast MGs exhibit smaller pop-ins under diamond-tip indentation, while annealed MGs exhibit bigger pop-ins[12,13]. Free volume has been identified as an explanation for annealing-induced embrittlement. MGs with different plastic responses have different free-volume concentrations ($\Delta x$)[14]. Free-volume annihilation rate $\Delta\dot{x}^-$ depends on environment[15,16], while free-volume creation rate $\Delta\dot{x}^+$ is both stress-dependent and $\Delta x$-sensitive[17]. As-cast MGs possess high $\Delta x$, resulting in low $\Delta\dot{x}^+$, while sub-$T_g$ annealing lowers $\Delta x$, leading to high $\Delta\dot{x}^+$[18]. An imbalance of rates, i.e., $\Delta\dot{x}^+ \gg \Delta\dot{x}^-$, is responsible for the loss of plasticity and therefore embrittlement.

However, embrittlement of as-spun MG ribbons while bending is a distinct phenomenon. Many as-spun MG ribbons break in seemingly elastic bending, that is, at bending strains smaller than the elastic limit[7]; despite calorimetry revealing an exotherm prior to $T_g$ on the heating curve, whose area reflects the enthalpy of relaxation ($\Delta H_{rel}$) proportional to $\Delta x$ (Ref. 19). Since the free-volume theory only applies to plasticity close to the yield stress ($\sigma_y$), there must be other structural changes taking place inside the apparently elastic range of MG ribbons that cause the embrittlement at low stresses. MGs can experience anelastic deformation at very small stresses and strains. For example, anelastic strain recovery was seen and continued for more than a year when a La-based MG was constrained at a bending strain of 0.25–0.5% via mandrel winding at room temperature[20,21]. Similarly, a Zr-based MG strained at 0.05% in compression showed stress relaxation over a 15-hour period, suggesting delayed structural relaxation and time-dependent mechanical response[22]. Furthermore, atomic-scale motion in a Zr-based MG under a compressive stress as low as $0.005\sigma_y$ was discovered by X-ray photon correlation spectroscopy, suggesting the presence of numerous reversible anelastic events alongside visco-plastic flow[23]. These findings imply that microscopic plastic flow can initiate at any stress level, but because the stiff elastic network applies a back stress to frustrated regions, which is compatible with anelastic behavior, such structural modifications should be recoverable[23]. It is necessary to have a thorough microscopic understanding of why MG anelasticity activates at such low stress levels.

The absence of a periodic atomic arrangement makes it difficult to detect microscopic defects in MG, even though their roles in embrittlement are prominent. The microscopic rearrangements in MGs before shear banding are conceptually described by Argon's shear transformation theory as an inelastic-strain producing event in which a compact cluster of atoms undergoes a cooperative, irreversible rearrangement from one metastable configuration to another under a local resolved shear stress, constituting the elementary unit of plastic deformation[24,25]. Shear transformation zones (STZs) are defined by Falk and Langer as pre-existing two-state Eshelby inclusions in a rigid matrix that, during creep, transition from circles to ellipses orientated either along or against the shear direction[26,27]. The stability of STZs is biased in favor of one orientation by applied stress, and they reverse directions when the load is removed[28]. An STZ yields in a particular direction but not when the loading direction rotates 90°, showing anisotropic activation in molecular-dynamics (MD) simulation[29]. The plastic response can even be polarized by quasi-elastic asymmetric mechanical cycling[30]. According to their findings, STZs in MGs differ from free volume in that they have a preferred angle to shear.

The shear transformations have been primarily investigated through temperature-varied creep-recovery experiment[31–33], where a pre-annealed MGs was heated to a temperature below $T_g$, loaded under stress for days, quenched to cryogenic temperatures and then unloaded. The dynamics of strain reversal were used as a probe of shear transformation. A spectrum of activation energy $W$ reflecting distinct atomic dynamics of these transformation events was produced by adjusting the high temperature and examining the ensuing change in recovery-strain rate[31]. High-temperature creep treatment induces structural anisotropy that enhances plasticity in bulk MGs, even reversing the embrittlement caused by structural relaxation[34]. However, because the applied high temperature would unavoidably eliminate quenched-in STZs in as-spun MGs, this method cannot be used to investigate them. Here, we investigate the room-temperature low-stress creep response of as-spun and annealed metallic-glass ribbons using stepwise and cyclic loading protocols. We find an anomalous non-monotonic creep response in the as-spun state, which is strongly suppressed after annealing. By combining mechanical measurements, structural characterization and MD simulations, we show that the full response can be consistently described by the competition between a finite pre-existing STZ population and a stress-activated STZ population. These results motivate an orientation-dependent framework for interpreting low-stress visco-elastic creep in metallic-glass ribbons, rather than a purely scalar description of STZ activity.

We therefore use room-temperature stress-varied creep-recovery experiments to avoid annealing at high temperatures. In stepwise creep, it is found that the creep strain initially falls and then increases; in cyclic creep, the creep strain is greater than the reversal strain in the first cycle. The dynamics of the quenched-in defects differ from those of the stress-activated ones, and the fact that they creep throughout a wide range of stress at low levels suggests a Schmid-like viscoelastic behavior linked to shear-resolved preferred orientation of STZs.

## Results

### Structural anisotropy in as-spun metallic glasses

Melt spinning, a directional process that involves severe shearing of the liquid cooling into the glassy state, produces structural anisotropy in as-spun MG ribbons[35]. The strain parallel to the length direction contracts twice as much as the strain parallel to the width direction after annealing[36–38]. The structure function $S(q)$ in ribbons varies in different directions according to X-ray and neutron scattering[39,40]. Small-angle neutron scattering suggests aligned defects may be related to shearing[41,42]. High-resolution transmission electron microscopy and an energy dispersive spectrometer confirmed that crystallinities and phase separation do not exist in our specimens (Fig. S1). Figure 1 presents the $I$ of $q$ of a $Zr_{65}Cu_{27.5}Al_{7.5}$ MG ribbon examined under selected area electron diffraction ($I$ for diffraction intensity, and $q$ for reciprocal vector). Here, azimuthal integrations over 5° centered on the ribbon length and width directions yields $I$. The first halo has peak positions ($q_1$) of 3.68 Å$^{-1}$ in the length direction and 3.74 Å$^{-1}$ in the width direction, indicating a 1.6% structural anisotropy. In contrast, following annealing at $0.9T_g$ for 96 hours, $q_1$ are 3.73 Å$^{-1}$ in the length direction and 3.74 Å$^{-1}$ in the width direction, indicating 0.4% structural anisotropy. The anisotropic diffraction signature observed in the as-spun ribbons, together with its substantial reduction after annealing, supports the presence of a frozen-in anisotropic glassy state[43]. Although these measurements do not directly image individual STZs, they are consistent with an orientational bias in the local structural environment that may facilitate direction-selective STZ activation under uniaxial loading.

### Stepwise creep of metallic glasses

We start by investigating the strain responses of MGs during stepwise creep. The $Mg_{68}Cu_{23}Gd_9$ (in atomic % hereafter) MG ribbons[22,44], about 33 μm thick, 1.04 mm wide and 40 mm long, were pulled under tensile stress ($\sigma$) that was incrementally increased after one-hour creep at each stress level (Fig. 2a). To stabilize the structure and minimize the influence of frozen-in stresses brought on by solidification from wheel and air sides[45], the ribbons made by melt spinning were aged for over a year at room temperature. Both the wheel and air sides of the ribbons

https://doi.org/10.1038/s41467-026-76196-x

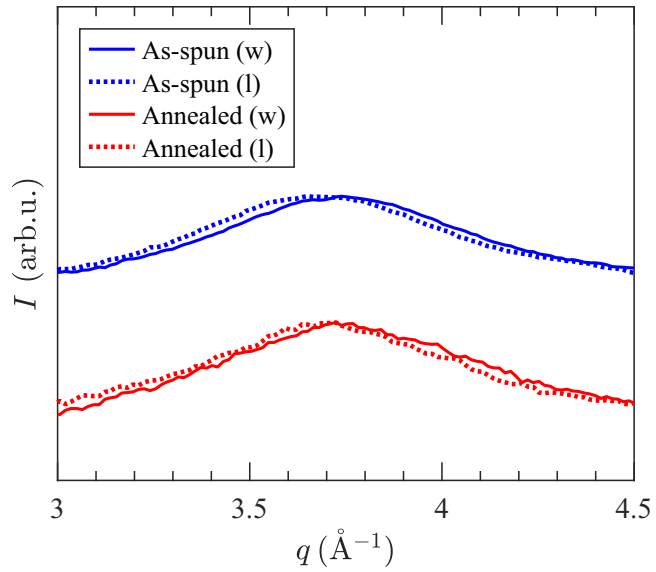


**Fig. 1 | The first diffraction-halo of a $Zr_{65}Cu_{27.5}Al_{7.5}$ metallic glass.** Here, $q$ is the reciprocal vector, and $I$ is intensity. Difference in the peak position of the first halo between the length (l) and width (w) directions is big for the as-spun but small for the annealed (at $0.9T_g$ for 96 hours). The curves are shifted vertically for clarification. Source data are provided as a Source Data file.

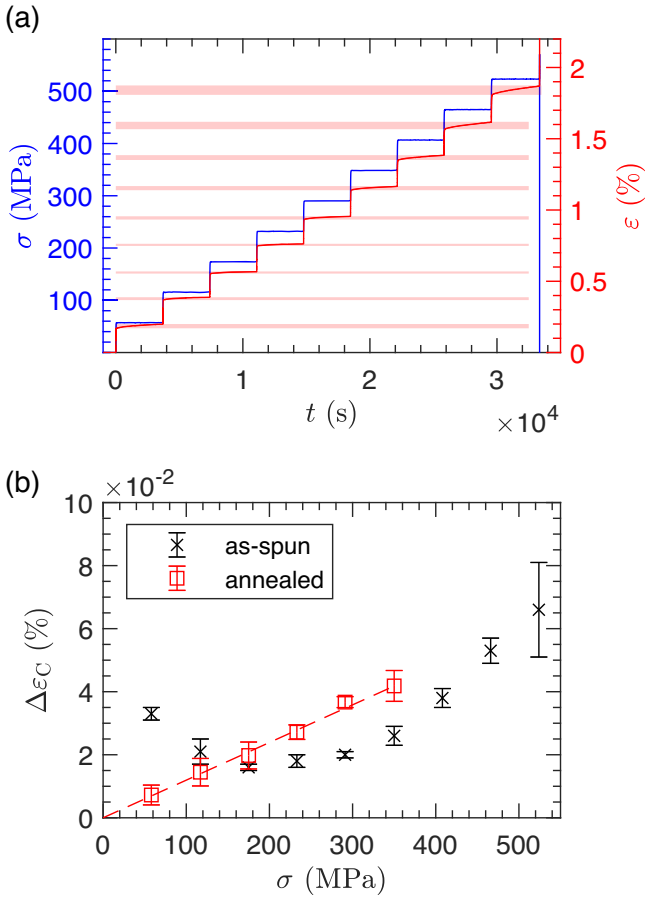


**Fig. 2 | Creep strain of the $Mg_{68}Cu_{23}Gd_9$ MG in stepwise creep. a** $\sigma$, $\varepsilon$ and $t$ represent stress, strain and time, respectively. Red-shaded bands highlight the creep-strain increment $\Delta\varepsilon_C$ after each one-hour creep. **b** $\Delta\varepsilon_C$ plotted against the incrementally added creep stress $\sigma$. Annealing was conducted at its $0.9T_g$ for an hour. The red-dashed line is a linear fit of $\Delta\varepsilon_C = 1.2 \times 10^{-4}\sigma$. Each test was repeated three times. The error bars represent standard deviation (SD). Source data are provided as a Source Data file.

have a mirror-like surface finish (Fig. S2a). The tension machine (IMMT 3, Tai-An Dai-Xuan Technology Company) with resolutions of 0.1 μm in displacement and 0.1 mN in force was used (details are given in the Supplementary Information). The specimen's length direction was carefully oriented along the axial direction of the machine before it was fixed by screwed anvils (Fig. S2b). Following all of our cyclic creep testing, no shear bands were found on the ribbon surfaces (Fig. S2c). Linear stress-strain response suggests that the specimen was straight (Fig. S2d). Room temperature is about 0.72 of its $T_g$ (= 419 K), and the interval between neighboring steps is 2 N (equivalent to 57 MPa). The increment in creep strain ($\varepsilon_C$) by the end of one-hour creep in each step ($\Delta\varepsilon_C$) is evaluated (as indicated by the red shadows in Fig. 2a). Rather unexpectedly, a non-linear $\sigma$-dependence of $\Delta\varepsilon_C$ was observed in the as-spun ribbon (Fig. 2b). $\Delta\varepsilon_C$ decreases as $\sigma$ increases in the first four steps ($\sigma$ = 57, 115, 175, 233 MPa). However, in the subsequent steps ($\sigma$ = 291, 350, 408, 466 and 524 MPa), $\Delta\varepsilon_C$ increases as $\sigma$ increases. Additionally, the "first-decline-then-rise" trend was eliminated if the same tests were performed on ribbons that had been annealed at $0.9T_g$ for an hour, and $\Delta\varepsilon_C$ increased linearly as $\sigma$ increased (Fig. 2b). Similar behaviors were observed on another $Zr_{65}Cu_{27.5}Al_{7.5}$ MG, of which the homologous temperature (test temperature relative to $T_g$) is only 0.47 (its $T_g$ = 636 K). As shown in Fig. S3, a distinct "first-decline-then-rise" trend of $\Delta\varepsilon_C$ to $\sigma$ was seen in its as-spun, but was lost in the annealed (pre-annealed at 90% of its $T_g$ for 96 hours).

A similar trend showed up in another $La_{30}Ce_{30}Ni_{10}Al_{20}Co_{10}$ MG (crept at 0.82 of its $T_g$), where the creep stress was added incrementally every 8 hours[33]. The accumulated creep strain $\Delta E_C$ (= $\sum_1^n \Delta\varepsilon_C$, $n$ = 3 and 6) of the $Mg_{68}Cu_{23}Gd_9$, if compared with $\Delta\varepsilon_C$ read from one-hour creep at 175 MPa and 350 MPa (See Fig. S4), corresponds well with each other, suggesting that the loading history does not change the total amount of creep strain at given stress if applied for more than an hour. These findings suggest that the "first-decline-then-rise" trend of $\Delta\varepsilon_C$ to stepwise creep is universal to MGs across a wide range of homologous temperatures.

## Cyclic creep of metallic glasses

Next, we investigate the strain responses of MGs during cyclic creep. The $Mg_{68}Cu_{23}Gd_9$ MG ribbon was subjected to a constant stress (both 175 MPa and 350 MPa were tested), crept for one hour, unloaded to zero and allowed to reverse for one hour. Four cycles of this loading-unloading procedure were performed (Fig. 3a). The strain responses during creep ($\varepsilon_C$) and reversal ($\varepsilon_R$) are compared. Figure 3b presents $\Delta\varepsilon_C$ and the amount of $\varepsilon_R$ reversed in one hour ($\Delta\varepsilon_R$) for the 1st-4th cycles. Increasing the creep stress does raise the $\Delta\varepsilon_C$ and $\Delta\varepsilon_R$ at any numbers of time interval ($\delta t$ = 1 h); however, it can be seen at both 175 MPa and 350 MPa that $\varepsilon_C$ decreases during the second cycle and remains almost constant throughout the subsequent cycles. Additionally, for the same creep stress, the 1-hour $\Delta\varepsilon_C$ values of the 2nd-4th cycles and the 1-hour $\Delta\varepsilon_R$ values of the 1st-4th cycles are almost identical. In fact, except for the 1st cycle, where $\varepsilon_R$ is always less than $\varepsilon_C$, $\varepsilon_C$ and $\varepsilon_R$ curves merge in the 2nd-4th cycles (See Fig. S5). Again, the facts that $\varepsilon_C > \varepsilon_R$ in the 1st cycle, and $\varepsilon_C = \varepsilon_R$ in further cycles were confirmed by using the $Zr_{65}Cu_{27.5}Al_{7.5}$ MG (See Fig. S4a). Additionally, $\varepsilon_C = \varepsilon_R$ in all four cycles when using the annealed specimens (Fig. S3c).

## Calorimetry of crept metallic glasses

Fast differential scanning calorimetry (FDSC, Mettler-Toledo FDSC 2+) experiments were conducted on the $Mg_{68}Cu_{23}Gd_9$ MG ribbons before and after creep. Specimens weighing a few nanograms were cut from the ribbons before creep or after creep in order to study the effects of strain reversal. Since the sample mass varies and is hard to determine, we use the fictive temperature ($T_f$) as a more robust metric for

https://doi.org/10.1038/s41467-026-76196-x

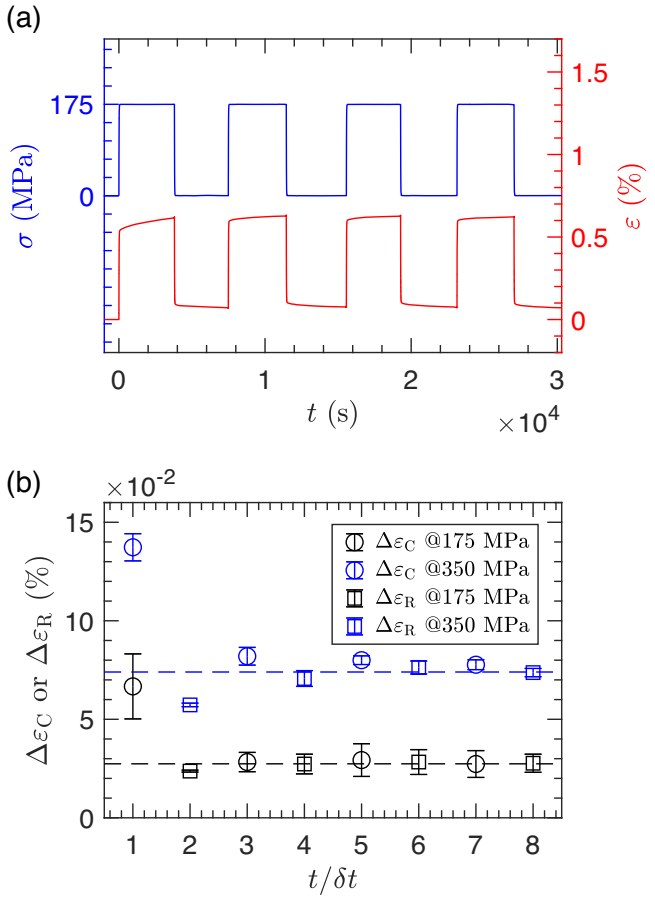


**Fig. 3 | Creep and reversal of the $Mg_{68}Cu_{23}Gd_9$ MG in cyclic creep. a** $\sigma$, $\varepsilon$ and $t$ represent stress, strain and time, respectively. **b** The amount of creep and reversal strains by the end of one-hour testing ($\Delta\varepsilon_C$ and $\Delta\varepsilon_R$), respectively, as a function of time ($t$). $\delta t$ of 1 h is the time interval. Each test was repeated three times. The error bars represent standard deviation (SD). Source data are provided as a Source Data file.

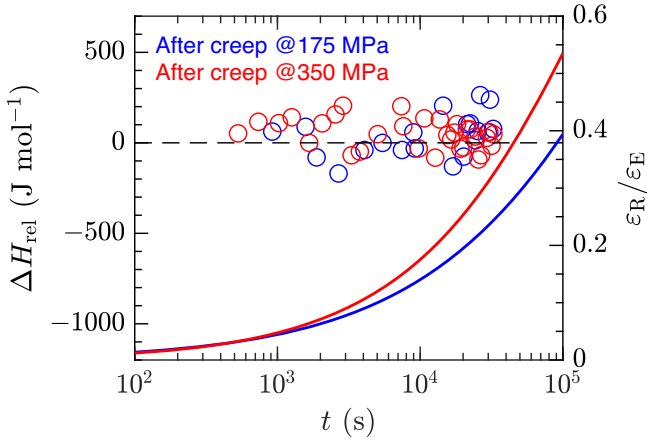


**Fig. 4 | Structural state of the $Mg_{68}Cu_{23}Gd_9$ MG before and after one-hour creep.** Left $Y$ axis: after creep, the relaxation enthalpy $\Delta H_{rel}$ (circles) remains unchanged with $t$. Each calorimetry measurement took less than 2 s. Dashed line denotes $\Delta H_{rel}$ of the as-spun ribbon. Right $Y$ axis: the reversal strain $\varepsilon_R$ normalized by the applied elastic-strain $\varepsilon_E$, as represented by the solid curves, increases with the increasing $t$. Source data are provided as a Source Data file.

comparing the thermal state of nanogram-scale samples[46], and relate it to the relaxation enthalpy through independent calorimetric calibration using differential scanning calorimetry (Perkin Elmer DSC 8000). Influence of thermal lag is carefully evaluated, which is found not severe at the heating rate ($\phi_h$) of 500 K $s^{-1}$. The $\Delta H_{rel}$ and $T_f$ of the as-spun MG at a $\phi_h$ of 20 K $min^{-1}$ (Fig. S6) are 1.1 J $mol^{-1}$ and 423 K, respectively, while $\Delta H_{rel}$ of the crept MGs are calculated by adding $\Delta C_p \Delta T_f$ to 1.1 J $mol^{-1}$. The specific heat-capacity change during glass transition, denoted by $\Delta C_p$, is 14.6 J $K^{-1}$ $mol^{-1}$ for $Mg_{68}Cu_{23}Gd_9$, and $\Delta T_f$ is the difference of $T_f$.

As shown in Fig. 4, $\Delta H_{rel}$ remains constant after creep at 175 MPa and 350 MPa. Additionally, $t$ has little effect on $\Delta H_{rel}$ during strain reversal. Although noticeable changes in $\varepsilon_R$ are observed (blue and red curves in Fig. 4), no discernible patterns in $\Delta H_{rel}$ are found with the increasing $t$ (Fig. 4). Even after 9 hours following the 1-hour creep at a given creep stress, $\Delta H_{rel}$ varies around the mean value. This indicates that the amount of $\varepsilon_R$ has no measurable effects on the $\Delta H_{rel}$ of MGs after creep. At 350 MPa, $\varepsilon_R/\varepsilon_E$ is only 0.0315 at $t$ = 530 s, much smaller than the $\varepsilon_R/\varepsilon_E$ of 0.319 at $t$ = 9 h. Within the sensitivity of the present FDSC analysis, we do not observe clear rejuvenation signatures after the creep-recovery protocol. Instead, the $\Delta H_{rel}$ remains nearly unchanged within experimental uncertainty, suggesting that the present low-stress visco-elastic response is not primarily governed by the rejuvenation pathway reported under other loading conditions[47–54]. Considering that most of the earlier treatments lasted longer than 24 hours and were conducted near their yield stress, this difference may reflect the distinct stress levels (below half the yield stress) and loading histories (one hour) involved.

## Molecular-dynamics simulation

A $Cu_{50}Zr_{50}$ MG with 108,000 total atoms was subjected to MD simulation. The equilibrium melt was rapidly cooled from 2000 K to 300 K over a 1 ns duration, followed by a 0.1 ns isothermal relaxation at 300 K to create the as-cast. The annealed sample preparation involved cooling from 2000 K to 800 K over 1 ns, isothermal relaxation at 800 K for 50 ns, cooling to 300 K over 1 ns, and followed by a final isothermal relaxation at 300 K for 1 ns. The annealing temperature 800 K is chosen because it is smaller than the nose-temperature of crystallization (837 K[55]) and $T_g$ (1000 K[56]). With a $t_C$ interval of 4 ns and a step magnitude $\Delta\sigma$ of 75 MPa, the sample was subjected to stepwise creep in tension. Details of the MD simulation are provided in the Supplementary Information. Fig. 4a displays the strain changes of the as-cast and annealed samples using the same protocol of stepwise creep. As seen in Fig. 2a, it is evident that the as-cast sample has a higher $\varepsilon_C$ than the annealed at the specified creep stress. Using the $\varepsilon$ difference between the end and the beginning of each creep step as $\Delta\varepsilon_C$ in simulation, we see a similar "first-decline-then-rise" tendency of $\Delta\varepsilon_C$ to the growing $\sigma$ for the as-cast, while $\Delta\varepsilon_C$ of the annealed increases modestly with the increasing $\sigma$ (Fig. 5b). Averaged non-affine displacement in the loading direction ($\overline{d}_{na,Z}$) firstly decreases and then gradually increases with the increasing $\sigma$ in the as-cast, while $\overline{d}_{na}$ of the annealed stays constantly (Fig. 5c). Thus, the large $\Delta\varepsilon_C$ at low stress (e.g. 75 MPa) is contributed by both a large number of non-affine activities and large non-affine displacements in the loading direction $\overline{d}_{na}$; the small $\Delta\varepsilon_C$ at medium stress (e.g. 375 MPa) is ascribed to reductions in both number and $\overline{d}_{na}$; the large $\Delta\varepsilon_C$ at high stress (e.g. 675 MPa) is associated with the increasing number of non-affine activities instead of $\overline{d}_{na}$. In contrast, the small $\Delta\varepsilon_C$ and $\overline{d}_{na}$ indicate very low non-affine activities in the annealed.

In order to gain a better understanding of the deformation mechanisms at the atomic scale, non-affine displacements of the atoms in the loading direction were visualized. The colors reflect the non-affine displacements in the loading direction, commencing at the start of each step and ending at the end of each step. Figs. 5d–f are projections of the atoms along the loading axis, and "d", "e", "f" represent the 1st, 5th and 9th loading steps of the as-cast, respectively, as indicated in Fig. 5a. Since the

https://doi.org/10.1038/s41467-026-76196-x

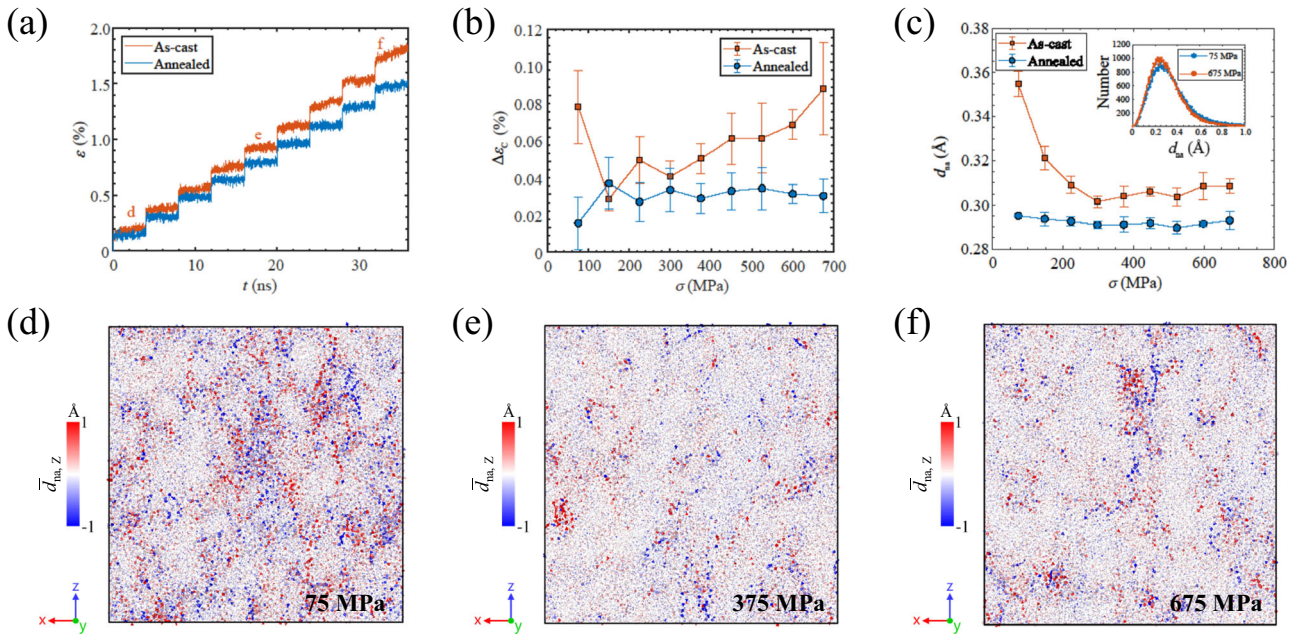


**Fig. 5 | Molecular-dynamics simulation of a $Cu_{50}Zr_{50}$ model MG under stepwise creep. a** The strain ($\varepsilon$) response to stepwise loading at a stress step of 75 MPa and creep time of 4 ns. Here, $t$ stands for time. **b** Averaged $\Delta\varepsilon_C$ plotted against the incrementally added creep stress $\sigma$. Duration of creep is 4 ns. The error bars represent standard deviation (SD). **c** Averaged non-affine displacements ($\overline{d}_{na}$) in the loading direction. The error bars represent standard deviation (SD). Inset: number distribution of $\overline{d}_{na}$ at 75 MPa and 675 MPa. All data in (**b**) and (**c**) come from the difference between the states after 4 ns following the stress increase and the initial one right after the stress increase. **d**–**f** Non-affine atomic displacements of the as-cast in Z axis (the loading direction) of the 1st, 5th, 9th steps projected on the X–Y planes. $\overline{d}_{na,Z}$ stands for the non-affine displacements in Z direction. The simulation was repeated five times with the same loading protocol. Source data are provided as a Source Data file.

colored atoms in Fig. 5d occupy a significant portion of the sample, it is evident that the non-affine atomic movements are active in the first step. On the other hand, as Fig. 5e illustrates, the non-affine occurrences are significantly reduced at the 5th step, where $\Delta\varepsilon_C$ is small. The non-affine displacements are re-activated in the final loading step (Fig. 5f). In comparison, the non-affine displacements of the annealed at any loading steps are small with fewer atoms involved (Fig. S7). Our simulation can also reproduce the cyclic-creep behaviors, where large non-affine activities are only seen in the first loading of the as-cast MG exhibiting the largest $\Delta\varepsilon_C$ (Fig. S8).

## Discussion

### Dynamics in strain reversal

The present work reports a non-linear $\sigma$-dependence of $\varepsilon_C$ (Fig. 2b). This kind of non-linearity differs from all previous results in that it is neither a deviation from $\varepsilon \propto \sigma$ nor a departure from $\dot{\varepsilon}_C \propto \sigma$. In monotonic loading of MGs, viscoelasticity causes $\varepsilon$ to be non-linear to $\sigma$ (Ref. 57). In stepwise loading, $\dot{\varepsilon}_C \propto \sigma$ would show $\Delta\varepsilon_C \propto \sigma$ at fixed $t_C$ (a monotonic increase of $\Delta\varepsilon_C$ with the increasing $\sigma$), which is not the case for the as-spun but is the case for the annealed (Fig. 2b), in line with previous findings examining pre-annealed MGs[32,58].

The above-mentioned results are consistent with a unified two-contribution description of the non-monotonic creep response. In this picture, the initial decrease reflects the progressive depletion of a finite quenched-in STZ population that is already present in the as-spun ribbons, whereas the subsequent increase arises from the growing contribution of stress-activated STZs as the applied stress increases. The annealed ribbons differ primarily in the greatly reduced contribution from the pre-existing STZ population, leading to an overall monotonic response. As described by Equation (1).

$$\Delta\varepsilon_C = \varepsilon_A N_A + \varepsilon_B N_B \quad (1)$$

where $N_A$ and $\varepsilon_A$ denote the number and 1h-strain of quenched-in STZs, while $N_B$ and $\varepsilon_B$ denote the number and 1h-strain of stress-activated STZs, this formulation avoids invoking separate mechanisms for different stress regimes and instead describes the full response through the stress-dependent balance between two physically distinct, but simultaneously present, contributions. It provides clues on why creep of as-spun MGs can begin at a much lower level within the elastic limit. Even if $\sigma$ is small, $\Delta\varepsilon_C$ is big because at the start of loading, $N_B = 0$ but $N_A \neq 0$. Stepwise creep causes quenched-in STZs to get depleted, which lowers $N_A$ and causes $\Delta\varepsilon_C$ to decrease. Conversely, at the start of stepwise loading, the annealed ribbons lost the significant $\Delta\varepsilon_C$ (Fig. 2) because annealing eliminated the quenched-in STZs from MG ribbons ($N_A \to 0$). The dynamics of the quenched-in and stress-activated STZs differ as well. The strain reverses as quickly as the creep strain develops in the 2nd-4th cycles of the as-spun (Fig. 3b) and in each cycle of the annealed (Figs. S3 and S5), suggesting that the reversal rate ($\dot{\varepsilon}_R$) equals the creep rate ($\dot{\varepsilon}_C$). According to the stress-activation scheme of STZs, the pre-annealed MGs exhibit equal time in creep and reversal ($t_R = t_C$)[32,58]. On the other hand, the strain creeps rather than reverses in the 1st cycle of the as-spun (Fig. 3b), displaying $\dot{\varepsilon}_R < \dot{\varepsilon}_C$ which denotes quenched-in STZs. Similar outcomes have been reported in several La-based as-spun MG ribbons: the strain reversal persisted for a year following a one-week creep by mandrel winding[20,21]. The findings indicate that quenched-in and stress-activated STZs are two distinct causes of MG viscoelasticity. In a recent MD simulation using a "frozen-atom" approach, anelastic deformation in MGs is found to be caused by unpredictable and transient cooperative motions of small groups of atoms outside the pre-existing structural defects[59], uncorrelated with soft spots assumed to correspond to shear transformation[25]. This is comparable to the behavior of stress-activated STZs, which are formed following stress activation. Actually, pre-existing soft spots (quenched-in STZs) are removed after annealing. Their work supports the theory that STZs in MGs have two origins.

Equation (2) takes the derivative of $\Delta\varepsilon_C$ of the initial creep to stress by

$$\frac{\partial\Delta\varepsilon_C}{\partial\sigma}=\frac{\partial\varepsilon_A}{\partial\sigma}N_A+\varepsilon_A\frac{\partial N_A}{\partial\sigma}+\frac{\partial\varepsilon_B}{\partial\sigma}N_B+\varepsilon_B\frac{\partial N_B}{\partial\sigma} \quad (2)$$

Firstly, calorimetry reveals no measurable change in $\Delta H_{rel}$ (Fig. 4), indicating that any stored rejuvenation associated with $N_A$ is below the calorimetric resolution (we approximate $\frac{\partial N_A}{\partial\sigma}\approx 0$ for the stored structural contribution resolved by calorimetry). Secondly, because $\dot{\varepsilon}_C=\dot{\varepsilon}_R$ for stress-activated STZs (Fig. 3), $\sigma$ plays no role in accelerating strain, indicating $\frac{\partial\varepsilon_B}{\partial\sigma}=0$. Thus, in the 2nd-4th cycles of the as-spun MG when only the stress-activated STZs contribute to the strain changes (Fig. 3b), $\frac{\partial\Delta\varepsilon_C}{\partial\sigma}$ is $\varepsilon_B\frac{\partial N_B}{\partial\sigma}$, only. Based on Fig. S5, $\varepsilon_B\frac{\partial N_B}{\partial\sigma}$ is about $3\times10^{-12}$ $Pa^{-1}$ for $Mg_{68}Cu_{23}Gd_9$. Since the value remains the same in the first cycle, $\frac{\partial\varepsilon_A}{\partial\sigma}N_A$ can be derived by its $\frac{\partial\Delta\varepsilon_C}{\partial\sigma}$ ($\approx 3.4\times10^{-12}$ $Pa^{-1}$) subtracting $\varepsilon_B\frac{\partial N_B}{\partial\sigma}$. For the as-spun $Mg_{68}Cu_{23}Gd_9$, $\frac{\partial\varepsilon_A}{\partial\sigma}N_A$ is $0.4\times10^{-12}$ $Pa^{-1}$. Our analysis suggests that quenched-in STZs in the as-spun MG ribbons made approximately 12% (=0.4/3.4) contribution to the total $\frac{\partial\Delta\varepsilon_C}{\partial\sigma}$.

### Schmid-like viscoelastic creep in metallic glasses

According to the relaxation model, STZ creep and recovery are thermal activation processes that necessitate overcoming an activation energy ($W$) barrier. The $W$-spectrum of STZs in pre-annealed MG ribbons has been resolved by Argon and Kuo using high-$T$ creep and low-$T$ recovery, ignoring the impact of $\sigma$[31]. Stress biasing was subsequently applied to $W$ using $W-\sigma\Omega$[60] or $W(1-\frac{\sigma}{\sigma_y})$[61]. Nevertheless, none of these can address our findings in the annealed and as-spun MGs (specified in the 2nd-4th cycles). If $W$ of the STZs in these samples is stress biased, then $W$ in recovery ($\sigma=0$) should be greater than that in creep ($\sigma\neq0$), resulting in $\dot{\varepsilon}_R<\dot{\varepsilon}_C$ instead of $\dot{\varepsilon}_R=\dot{\varepsilon}_C$ (Figs. 4a and S3). For this reason, we find stress-activated STZs that are typical of both $\sigma$-independent and $T$-dependent $W$. Additionally, $\Delta\varepsilon_C$ of the stress-activated STZs, such as in annealed MGs, depends on $\frac{\partial N_B}{\partial\sigma}$ rather than $\frac{\partial\varepsilon_B}{\partial\sigma}$, indicating that they creep immediately after creation or in other words, creep stress is less than activation stress.

We now focus on the spectrum of $W$ associated with the quenched-in STZs. All of the current models imply that biasing of $W$ would happen at high $\sigma$. Since we find a significant $\varepsilon_C$ at $\sigma$ as low as 57 MPa, the spectrum must peak at a modest $W$. The cooperative shear model[61] states that the biasing to $W$ is $(1-\frac{\sigma}{\sigma_y})^{\frac{3}{2}}\approx0.88$. Since the test was conducted at room temperature and the exponential component in rate dynamics is $e^{-\frac{W}{RT}}$, a 12% drop of $W$ is comparable to a 14% rise of $T$ ($1.14=\frac{1}{0.88}$), i.e., 342 K. This means that a small thermal fluctuation would result in a significant change in creep and a big scatter of data. Additionally, if $\sigma$ = 175 MPa and $(1-\frac{\sigma}{\sigma_y})^{\frac{3}{2}}\approx0.65$, the equivalent temperature approaches 462 K (=1.1$T_g$), indicating a uniform shape change and Newtonian flow. They are not all seen.

This thus motivates us to consider a Schmid-like framework for STZs with orientation-sensitive creep. Polycrystalline metals have a wide range of $\sigma_y$. Schmid's law states that the critical resolved shear stress ($\tau$) needed to move dislocations along any slip planes is the same, but the normal stress $\sigma$ required to activate dislocation-slip depends on $\sigma=\frac{\tau}{m}$, where $m=\cos\theta\cos\phi$ with $\theta$ the angle between the normal stress and the plane normal and $\phi$ the angle between in-plane slip direction and the normal stress[62]. The lesson is that even if $\tau$ is the same, grain orientation affects $\sigma$ a lot. Unlike dislocation slip, STZ activation in MGs does not require slip-plane normal to be perpendicular to the slip direction, and hence $m\in[-0.5, 0.5]$ is not directly applicable. Instead $|m|\in[0, 1]$, $\sigma\in[\tau, +\infty]$. Many MD simulations have demonstrated that STZs exhibit preferential orientations to shear[29,30], and many experiments have shown structural anisotropy[36–42] that is closely related to this microscopic origin. Consequently, the orientations of STZs may considerably change their creep stress even if $\tau$ is similarly small. Low-$\sigma$ creep is possible because the yield criterion is no longer constrained by $\sigma=2\tau$ as for shear banding[57]. Stepwise adding $\sigma$ would exhaust the available $m$ given a small $\tau$ for the quenched-in STZs, resulting in a drop of $\Delta\varepsilon_C$ (Fig. 2b).

Heterogeneity has long been recognized in MGs, which would certainly widen the $W$ distribution of STZs. According to $\tau=\frac{q}{2}$, Fig. 2b from the stepwise creep could reflect the $W$ spectrum. Because the cooperative shear model multiplies the activation energy $W$ by a bias of $(1-\frac{\sigma}{\sigma_y})$, $\Delta\varepsilon_C$ should be higher at high $\sigma$ than at low $\sigma$[61]. In this instance, the question is not the scatter of $W$ but rather the reason why creep of MGs has a low-$\sigma$ peak together with annealing dependence and cyclic asymmetry (Figs. 2 and 3). Density or chemical fluctuations are the likely source of heterogeneity in MGs, but are unlikely to result in two-phase structure and hence bimodality. No crystallites were observed under high-resolution transmission electron microscopy (Fig. S1), and no phase separation was detected by energy-dispersive spectroscopy, indicating that the variations are inherent. Introducing an orientation factor transforms the apparent activation stress from $\sigma=2\tau$ to $\sigma=\frac{\tau}{m}$ ($m\in[0,1]$), allowing STZs with comparable intrinsic $\tau$ to be activated over a broader external-stress range. For this reason, we suggest an orientation-dependent, Schmid-like framework for STZs that explains why the spectrum of quenched-in STZs peaks at low $\sigma$ but not at high $\sigma$.

Defect specification in metallic glasses remains a great challenge because of their long-range disordered atomic structure. The current study clarified two kinds of shear transformation zones in as-spun metallic glasses by testing with tensile creep loading techniques. The distinction is based on i) a first-decrease-then-increase trend of the creep strain in the as-spun upon stepwise creep, and ii) whether or not stress speeds up the dynamics in creep and reversal. Creep strain in annealed metallic glasses increases monotonically upon stepwise creep and reverses as quickly as it creeps under load following stress removal. Fast differential scanning calorimetry shows no measurable relaxation-enthalpy change of the metallic glass following creep within the present sensitivity, and molecular-dynamics simulation finds significant non-affine atomic activities when creep stress is near and far from the yield stress. The mechanical measurements, structural characterization and molecular-dynamics simulations consistently support a unified picture in which the observed response arises from the competition between a finite quenched-in STZ population and a stress-activated STZ population. The findings provide evidence for an orientation-dependent framework for interpreting low-stress viscoelastic creep in metallic-glass ribbons. More broadly, they highlight how frozen-in structural anisotropy can shape the mechanical response of glassy solids far below yielding.

## Methods

Metallic glass (MG) composition $Mg_{68}Cu_{23}Gd_9$ (in at. % hereafter) and $Zr_{65}Cu_{27.5}Al_{7.5}$ were selected for this study. Ribbons about 33 μm thick and 1.04 mm wide for the Mg-based and 31 μm thick and 1.02 mm wide for the Zr-based were obtained. Ribbons aged for 1–1.5 years were studied to minimize the risks of room-temperature aging of as-spun Mg-based MGs, which stabilize structurally and property-wise. The glass-transition temperature $T_g$ of 419 K (for the Mg-based) and 636 K (for the Zr-based) was determined at a heating rate ($\phi_h$) of 20 K $min^{-1}$ using a differential scanning calorimeter (Perkin Elmer DSC 800). Annealing was conducted in a vacuum furnace at their 0.9$T_g$ for 1 hour for the $Mg_{68}Cu_{23}Gd_9$, and for 96 hours for the $Zr_{65}Cu_{27.5}Al_{7.5}$ MGs. The amorphicity of the ribbons was confirmed on both sides using X-ray diffraction, using a lab X-ray diffractor (Bruker D8 Advance) with Cu-K$\alpha$ radiation. High-resolution transmission electron microscopy (JEOL JEM-2100Plus 200 kV) images were captured on $Zr_{65}Cu_{27.5}Al_{7.5}$ MGs, where no crystallites are seen. A custom-built tensile-testing apparatus

(IMMT 3, Tai-An Dai-Xuan Technology Company) was employed in this study. Tensile loading was achieved by a two-stage gear-reduction motor that pulled the ribbons at a constant speed of 500 mN $s^{-1}$ to a designated load. The load was measured by a load cell (Bengbu Dayang Sensor Systems Engineering Company), ranging from 0 to 200 N with a resolution of 100 mN. The displacement of the sample was recorded by a grating ruler (Chengdu Ditron Opto-Electronics Equipment Company) with a travel distance exceeding 5 cm and a resolution of 0.1 µm. The data acquisition system had a time resolution of 33 ms. The stress ($\sigma$) was calculated by dividing the load by the ribbon cross-sectional area ($3.43 \times 10^{-8}$ $m^2$), while strain ($\varepsilon$) was calculated by dividing the recorded displacement by the sample length (20 mm). UFH high-temperature sensors were used in the fast differential scanning calorimetry (FDSC, Mettler-Toledo FDSC 2+) experiments at a heating rate $\phi_h$ of 500 K $s^{-1}$.

All molecular-dynamics simulations were performed using the LAMMPS software package. Atomic interactions were modeled using an embedded-atom method (EAM) potential specifically parameterized for Cu-Zr systems. The simulation cell contained a total of 108,000 atoms with equal proportions of copper (54,000 atoms) and zirconium (54,000 atoms). Simulations employed an NPT ensemble (constant number of particles, pressure, and temperature) with periodic boundary conditions applied in all three dimensions. Two distinct sample preparation protocols were implemented to generate initial configurations with different relaxation states. For both protocols, samples were first equilibrated at 2000 K for 1 ns to ensure homogeneity above the melting temperature. The as-cast was subsequently cooled linearly from 2000 K to 300 K over a 1 ns duration, followed by a brief isothermal relaxation period of 0.1 ns at 300 K before saving the configuration for tensile testing. The annealed sample was prepared by cooling from 2000 K to 800 K over 1 ns, followed by an extended isothermal relaxation at 800 K for 50 ns to achieve enhanced structural relaxation. This sample was then cooled to 300 K over 1 ns and subjected to a final isothermal relaxation at 300 K for 1 ns before being saved for subsequent tensile tests. Two distinct tensile testing protocols were performed on both sample types at room temperature (300 K). The stepwise-creep test was performed by incrementally increasing the stress along the Z axis, with a step magnitude of 75 MPa and stress holding for 4 ns. This protocol continued through nine sequential steps, reaching a maximum stress of 675 MPa. The cyclic loading/unloading tensile test employed a constant creep stress of 500 MPa during loading, with each 4 ns holding period followed by a 4 ns unloading period at zero applied stress. This loading/unloading cycle was repeated four times, resulting in a total simulation duration of 32 ns. During all tensile simulations, lateral dimensions were permitted to relax under zero pressure constraints while maintaining constant temperature conditions.

## Data availability

All data generated or analyzed during this study are included in this published article (and its supplementary information files). Source data are provided with this paper.

## References


1. Ashby, M. F. & Greer, A. L. Metallic glasses as structural materials. *Scr. Mater.* **54**, 321–326 (2006).
2. McHenry, M. E., Willard, M. A. & Laughlin, D. E. Amorphous and nanocrystalline materials for applications as soft magnets. *Prog. Mater. Sci.* **44**, 291–433 (1999).
3. Silveyra, J. M., Ferrara, E., Huber, D. L. & Monson, T. C. Soft magnetic materials for a sustainable and electrified world. *Science* **362**, eaao0195 (2018).
4. Li, H.-X., Lu, Z.-C., Wang, S.-L., Wu, Y. & Lu, Z.-P. Fe-based bulk metallic glasses: glass formation, fabrication, properties and applications. *Prog. Mater. Sci.* **103**, 235–318 (2019).
5. Li, X. et al. Exceptionally high saturation magnetic flux density and ultralow coercivity via an amorphous-nanocrystalline transitional microstructure in an FeCo-based alloy. *Adv. Mater.* **35**, 2205863 (2023).
6. Enomoto, Y., Suzuki, K., Okita, S., Eto, K. & Katayama, E. Evaluation of a motor with an amorphous iron core punched by a die. *IEEJ J. Ind. Appl.* **10**, 785–792 (2021).
7. Wu, T. W. & Spaepen, F. The relation between embrittlement and structural relaxation of an amorphous metal. *Philos. Mag. B* **61**, 739–750 (1990).
8. Kumar, G., Neibecker, P., Liu, Y. H. & Schroers, J. Critical fictive temperature for plasticity in metallic glasses. *Nat. Commun.* **4**, 1536 (2013).
9. Yang, G. N. et al. Serration behaviours in metallic glasses with different plasticity. *Philos. Mag.* **96**, 2243–2255 (2016).
10. Dalla Torre, F. H., Klaumünzer, D., Maaß, R. & Löffler, J. F. Stick-slip behavior of serrated flow during inhomogeneous deformation of bulk metallic glasses. *Acta Mater.* **58**, 3742–3750 (2010).
11. Ramamurty, U., Lee, M. L., Basu, J. & Li, Y. Embrittlement of a bulk metallic glass due to low-temperature annealing. *Scr. Mater.* **47**, 107–111 (2002).
12. Murali, P. & Ramamurty, U. Embrittlement of a bulk metallic glass due to sub-TG annealing. *Acta Mater.* **53**, 1467–1478 (2005).
13. Chen, Y. et al. Nanoindentation reveals universal scaling of pop-in plasticity in metallic glasses. *Scr. Mater.* **259**, 116549 (2025).
14. Chen, L. Y. et al. Free-volume-induced enhancement of plasticity in a monolithic bulk metallic glass at room temperature. *Scr. Mater.* **59**, 75–78 (2008).
15. Jin, H. J., Gu, X. J., Wen, P., Wang, L. B. & Lu, K. Pressure effect on the structural relaxation and glass transition in metallic glasses. *Acta Mater.* **51**, 6219–6231 (2003).
16. Wang, Z. T., Pan, J., Li, Y. & Schuh, C. A. Densification and strain hardening of a metallic glass under tension at room temperature. *Phys. Rev. Lett.* **111**, 135504 (2013).
17. Wei, Y. et al. Accelerating structural relaxation of shear band at ambient conditions through cryogenic thermal-cycling. *Sci. China Mater.* **67**, 974–982 (2024).
18. Spaepen, F. A microscopic mechanism for steady state inhomogeneous flow in metallic glasses. *Acta Metall.* **25**, 407–415 (1977).
19. Slipenyuk, A. & Eckert, J. Correlation between enthalpy change and free volume reduction during structural relaxation of $Zr_{55}Cu_{30}Al_{10}Ni_5$ metallic glass. *Scr. Mater.* **50**, 39–44 (2004).
20. Lei, T. J. et al. Microscopic characterization of structural relaxation and cryogenic rejuvenation in metallic glasses. *Acta Mater.* **164**, 165–170 (2019).
21. Lei, T. J. et al. Composition dependence of metallic glass plasticity and its prediction from anelastic relaxation — a shear transformation zone analysis. *Acta Mater.* **195**, 81–86 (2020).
22. Chen, Y., Sun, Y. H. & Wang, W. H. Understanding the stretched exponential decay of strained metallic glasses by a free-volume model. *Phys. Rev. B* **110**, 1344309 (2024).
23. Riechers, B., Das, A., Rashidi, R., Dufresne, E. & Maaß, R. Metallic glasses: elastically stiff yet flowing at any stress. *Mater. Today* **82**, 92–98 (2025).
24. Argon, A. S. Mechanisms of inelastic deformation in metallic glasses. *J. Phys. Chem. Solids* **43**, 945–961 (1982).
25. Argon, A. S. Strain avalanches in plasticity. *Philos. Mag.* **93**, 3795–3808 (2013).
26. Falk, M. L. & Langer, J. S. Dynamics of viscoplastic deformation in amorphous solids. *Phys. Rev. E* **57**, 7192–7205 (1998).
27. Falk, M. L. & Langer, J. S. Thermal effects in the shear-transformation-zone theory of amorphous plasticity: Comparisons to metallic glass data. *Phys. Rev. E* **70**, 011507 (2004).

28. Costa, M. B. & Greer, A. L. Enthalpy of anelasticity and rejuvenation of metallic glasses. *Acta Mater.* **265**, 119609 (2024).
29. Shang, B., Wang, W. & Guan, P. Cycle deformation enabled controllable mechanical polarity of bulk metallic glasses. *Acta Mater.* **225**, 117557 (2022).
30. Xu, B., Falk, M. L., Patinet, S. & Guan, P. Atomic nonaffinity as a predictor of plasticity in amorphous solids. *Phys. Rev. Mater.* **5**, 025603 (2021).
31. Argon, A. S. & Kuo, H. Y. Free energy spectra for inelastic deformation of five metallic glass alloys. *J. Non-Cryst. Solids* **37**, 241–266 (1980).
32. Taub, A. I. & Luborsky, F. E. Creep, stress relaxation and structural change of amorphous alloys. *Acta Metall.* **29**, 1939–1948 (1981).
33. Qiao, J. C., Pelletier, J. M. & Yao, Y. Creep in bulk metallic glasses. transition from linear to nonlinear regime. *Mater. Sci. Eng. A* **743**, 185–189 (2019).
34. Tong, Y. et al. Recovering compressive plasticity of bulk metallic glasses by high-temperature creep. *Scr. Mater.* **69**, 570–573 (2013).
35. Miller, C. E. & Chen, H. S. A rapid quenching technique for the preparation of thin uniform films of amorphous solids. *Rev. Sci. Instrum.* **41**, 1237 (1970).
36. Sinning, H. R., Leonardsson, L. & Cahn, R. W. Irreversible anisotropic length changes in $Fe_{40}Ni_{40}B_{20}$ and a search for reversible length changes in several metallic glasses. *Int. J. Rapid Solidif.* **1**, 175–197 (1985).
37. Huizer, E. & Van Den Beukel, A. Reversible and irreversible length changes in amorphous $Fe_{40}Ni_{40}B_{20}$ during structural relaxation. *Acta Metall.* **35**, 2843–2850 (1987).
38. Friedrichs, H. & Neuhauser, H. Study of structural relaxation of metallic glasses by stress-free dilatometry. *J. Phys.: Condens. Matter* **1**, 8305 (1989).
39. Windsor, C. G., Boudreaux, D. S. & Narasimhan, M. C. A search for anisotropy in the structure factor of amorphous $Pd_{0.8}Si_{0.2}$ ribbon. *Phys. Lett. A* **67**, 282–284 (1978).
40. Spilsbury, D., Butvin, P., Cowlam, N., Howells, W. S. & Cooper, R. J. Some evidence for 'directional atomic pair ordering' in a cobalt-based metallic glass. *Mater. Sci. Eng. A* **226–228**, 187–191 (1997).
41. Yavari, A. R. & Desre, P. Substrate-induced liquid shearing and defect anisotropy in metallic glasses. *J. Phys. F: Met. Phys.* **14**, 291 (1984).
42. Steeb, S. & Lamparter, P. Recent structural results with amorphous-alloys using neutron-diffraction. *J. Phys. (Paris)* **46**, 247–253 (1985).
43. Suzuki, Y., Haimovich, J. & Egami, T. Bond-orientational anisotropy in metallic glasses observed by X-ray diffraction. *Phys. Rev. B* **35**, 2162–2168 (1987).
44. Chen, Y., Bo, Z.-X., Sun, Y. H., Sun, B.-A. & Wang, W. H. Pre-yield serrations in a Mg-based bulk metallic glass during compression. *J. Alloy. Compd.* **945**, 169268 (2023).
45. Castellero, A., Moser, B., Uhlenhaut, D. I., Dalla Torre, F. H. & Löffler, J. F. Room-temperature creep and structural relaxation of Mg-Cu-Y metallic glasses. *Acta Mater.* **56**, 3777–3785 (2008).
46. Yue, Y. Z., Christiansen, J. D. & Jensen, S. L. Determination of the fictive temperature for a hyperquenched glass. *Chem. Phys. Lett.* **357**, 20–24 (2002).
47. Lee, S.-C., Lee, C.-M., Yang, J.-W. & Lee, J.-C. Microstructural evolution of an elastostatically compressed amorphous alloy and its influence on the mechanical properties. *Scr. Mater.* **58**, 591–594 (2008).
48. Lee, J.-C. Calorimetric study of $\beta$-relaxation in an amorphous alloy: an experimental technique for measuring the activation energy for shear transformation. *Intermetallics* **44**, 116–120 (2014).
49. Park, K.-W. et al. Elastostatically induced structural disordering in amorphous alloys. *Acta Mater.* **56**, 5440–5450 (2008).
50. Lee, S.-C. et al. Structural disordering process of an amorphous alloy driven by the elastostatic compression at room temperature. *Appl. Phys. Lett.* **92**, 1519006 (2008).
51. Greer, A. L. & Sun, Y. H. Stored energy in metallic glasses due to strains within the elastic limit. *Philos. Mag.* **96**, 1643–1663 (2016).
52. Samavatian, M., Gholamipour, R., Amadeh, A. A. & Mirdamadi, S. Extra rejuvenation of $Zr_{55}Cu_{30}Al_{10}Ni_5$ bulk metallic glass using elastostatic loading and cryothermal treatment interaction. *J. Non-Cryst. Solids* **506**, 39–45 (2019).
53. Cui, J., Luo, Q., Di, S., Zhang, Z. & Shen, B. Rejuvenation-to-relaxation transition induced by elastostatic compression and its effect on deformation behavior in a Zr-based bulk metallic glass. *Metals* **12**, 282 (2022).
54. Sohrabi, S. et al. Rejuvenation by compressive elasto-static loading: the role of static stress on a Zr-based metallic glass. *J. Alloy. Compd.* **933**, 167715 (2023).
55. Puosi, F. & Pasturel, A. Nucleation kinetics in a supercooled metallic glass former. *Acta Mater.* **174**, 387–397 (2019).
56. Lu, T. et al. 1.7 times thermal expansion from glass to liquid. *Acta Mater.* **242**, 118450 (2023).
57. Schuh, C. A., Hufnagel, T. C. & Ramamurty, U. Mechanical behavior of amorphous alloys. *Acta Mater.* **55**, 4067–4109 (2007).
58. Perez, J., Fouquet, F. & He, Y. Homogeneous flow in metallic glasses. *Phys. Status Solidi A* **72**, 289–300 (1982).
59. Shiihara, Y., Iwashita, T., Adachi, N., Todaka, Y. & Egami, T. Cooperative atomic motion during shear deformation in metallic glass. *Nat. Commun.* **17**, 1604 (2026).
60. Tönnies, D., Samwer, K., Derlet, P. M., Volkert, C. A. & Maaß, R. Rate-dependent shear-band initiation in a metallic glass. *Appl. Phys. Lett.* **106**, 171907 (2015).
61. Johnson, W. L. & Samwer, K. A universal criterion for plastic yielding of metallic glasses with a $(t/T_g)^{2/3}$ temperature dependence. *Phys. Rev. Lett.* **95**, 195501 (2005).
62. Schmid, E. & Boas, W. *Plasticity of Crystals with Special Reference to Metals; A Translation from the German by F. A. Hughes & Co., Limited, London*. (F. A. Hughes & Co., Limited, 1950).


## Acknowledgements

The authors are grateful for their useful discussions with Prof. C. Robert E. Maaß and Dr. Birte Riechers from the Federal Institute of Materials Testing and Research (BAM) in Germany, Prof. A. Lindsay Greer from University of Cambridge in the United Kingdoms, Prof. P. F. Guan from Ningbo Institute of Materials Technology and Engineering Chinese Academy of Sciences in China, and Prof. M. Q. Jiang from Institute of Mechanics Chinese Academy of Sciences in China.

## Author contributions

Y.C. designed and fabricated the tension machine, prepared the specimens, and performed the tensile tests. X.L. conducted the differential scanning calorimetry tests. X.D. annealed the specimens, conducted mechanical tests and performed the electron microscopy experiments. S.L.L. designed the Molecular-dynamics simulation and performed their statistical analysis. W.W. provided facilities and supervised the project. Y.H.S. led the observations and analysis, acquired the funding, and wrote the manuscript. All authors read and approved the final manuscript. Correspondence and requests for materials should be addressed to S.L.L. (liusl95@outlook.com) and Y.H.S. (ysun58@iphy.ac.cn).

## Funding

This work was supported by the National Natural Science Foundation of China (92580120, 52471188) and the Talent Hub for "AI+ New Materials" Basic Research.

## Competing interests

The authors declare no competing interests.

## Additional information

**Supplementary information** The online version contains supplementary material available at https://doi.org/10.1038/s41467-026-76196-x.

**Correspondence** and requests for materials should be addressed to Song Ling Liu or Yong Hao Sun.

**Peer review information** *Nature Communications* thanks Jichao Qiao and the other anonymous reviewer(s) for their contribution to the peer review of this work. A peer review file is available.